Nonlinear Processes in Geophysics (1994) 1:31 - 40

Nonlinear Processes in Geophysics

Periodic and homoclinic orbits in a toy climate model

M. Toner[1] and A.D. Kirwan, Jr.[2]

[1] Dept. of Mathematics and Statistics, Old Dominion University, Norfolk, Virginia, USA
[2] Center for Coastal Physical Oceanography, Old Dominion University, Norfolk, Virginia, USA

Received 20 December 1993 - Accepted 1 March 1994 - Communicated by A.R. Osborne

Abstract. A two dimensional system of autonomous nonlinear ordinary differential equations models glacier growth and temperature changes on an idealized planet. We apply standard perturbative techniques from dynamical systems theory to study small amplitude periodic orbits about a constant equilibrium. The equations are put in cononical form and the local phase space topology is examined. Maximum and minimum periods of oscillation are obtained and related to the radius of the orbit. An adjacent equilibrium is shown to have saddle character and the inflowing and outflowing manifolds of this saddle are studied using numerical integration. The inflowing manifolds show the region of attraction for the periodic orbit. As the frequency gets small, the adjacent (saddle) equilibrium approaches the radius of the periodic orbit. The bifurcation of the periodic orbit to a stable homoclinic orbit is observed when an inflowing manifold and an outflowing manifold of the adjacent equilibrium cross.

1 Introduction

Since the pioneering work of Lorenz in the early 1960's toy models have played an important role in both geophysics and dynamical systems. The idea behind toy models is appealing. By considering an idealized planet with a restricted number of physical processes, insight may be gained into how the processes interact. Toy climate models, for example, have been used as "sanity checks" for the results from primitive equation based climate simulations.

Mathematically the model takes the form of a two dimensional nonlinear ordinary differential equation relating the annual average radiation temperature of a planet to the fraction of the planet's surface that is glaciated. Introduced in Posmentier (1990), this model has numerically demonstrated periodic, period doubling, quasiperiodic, chaotic and catastrophic solutions. The more complicated solutions were obtained by perturbing the linear part of the autonomous equations with periodic time dependence.

In this paper, we simplify the model by considering an autonomous formulation and examine the types of invariant manifolds that are produced. The idea behind this approach is to study the long time behavior of solutions initially in various neighborhoods of phase space. Analytic approximations may be used to determine some of these manifolds, so parameter interplay may be related to phase dynamics.

The model is introduced in Sect. 2. A constant equilibrium temperature/glaciation is chosen in Sect. 3 and other equilibria are discussed. In Sect. 4, Poincare-Andronov-Hopf bifurcation is used to obtain a periodic orbit encircling the chosen equilibrium. An adjacent constant equilibrium is determined in Sect. 5 and shown to have saddle character. Minimum and maximum frequencies of the periodic orbit and deviations from the chosen equilibrium are discussed in Sect. 6. Numerical solutions demonstrating the bifurcation of the periodic orbit to a homoclinic orbit are given in Sect. 7.

2 Formulation

The following equations represent the model:

$$\begin{aligned} \dot{G} &= RG(1-G) - AG - BT + C \\ \dot{T} &= L\dot{G} - KT^4 + F(1-G). \end{aligned} \tag{1}$$

Here G is the percent of the planet surface covered by glaciation and T is the average radiation temperature of the planet. Although the model does not account for geographic variability or the presence of an ocean it does account for a number of physical processes that are believed to be important in climate fluctuations.

The first term in the function for $\dot{G}$ accounts for the portion of the total planetary evaporation that falls on

Correspondence to: M. Toner

the glacier, thus contributing to its growth. The parameter R is proportional to the evaporation rate. The term AG accounts for enhanced melting when the glacier grows and advances towards the equator. Next, BT accounts for the balance between enhanced melting and increased precipitation when the temperature rises. For $B > 0$ the melting dominates and $B < 0$ the precipitation dominates. The constant C is used as a planetary constant and will be determined by choosing an equilibrium temperature. The parameters A, B, C will be considered soft and used to tune the model.

In the equation for $\dot{T}$, the first term $L\dot{G}$ accounts for warming associated with latent heat released by growth of the glacier. The parameter L is proportional to the latent heat of evaporation. The long-wave black body radiation leaving the planet is accounted for by KT^4 with K being proportional to the black-body emissivity. Absorption of short-wave radiation by the non-glaciated portion of the planet is represented by $F(1-G)$ with F being proportional to the albedo of the bare planet surface.

3 Equilibrium solutions

The simplest solutions of (1) are values of G and T where $\dot{G} = \dot{T} = 0$. While physically rather uninteresting, equilibrium solutions provide a mathematical template of phase flow. Locating such points and determining the stability of each provides neighborhoods in phase space where solutions have predictable behavior. In this section we choose an equilibrium with the soft parameter C in (1).

To locate constant equilibrium solutions we observe that (1) may be written as

$$\begin{bmatrix} 1 & 0 \\ -L & 1 \end{bmatrix} \begin{bmatrix} \dot{G} \\ \dot{T} \end{bmatrix} = \begin{bmatrix} RG(1-G) - AG - BT + C \\ -KT^4 + F(1-G) \end{bmatrix}. \tag{2}$$

One root of the right hand side of (2) may be chosen using the constant C as follows. First substitute

$$G = 1 - \kappa T^4 \tag{3}$$

where we have written

$$K = \kappa F \tag{4}$$

for convience. Then we solve

$$-R\kappa^2 T^8 + (A\kappa + R\kappa)T^4 - BT + C - A = 0. \tag{5}$$

We may choose an equilibrium temperature T_e by setting

$$C = R\kappa^2 T_e^8 - (R\kappa + A\kappa)T_e^4 + BT_e + A \tag{6}$$

With this choice of C, we factor (5) to obtain

$$\begin{aligned}(T - T_e)\{&-R\kappa^2 T^7 - T_e R\kappa^2 T^6 - T_e^2 R\kappa^2 T^5 \\ &-T_e^3 R\kappa^2 T^4 + \kappa\left(R - R\kappa T_e^4 + A\right)T^3 \\ &+T_e\kappa\left(R - R\kappa T_e^4 + A\right)T^2 \\ &+T_e^2\kappa\left(R - R\kappa T_e^4 + A\right)T \\ &-R\kappa^2 T_e^7 + T_e^3 A\kappa + T_e^3 R\kappa - B\} = 0.\end{aligned} \tag{7}$$

Other equilibria must be roots to the above seventh order polynomial which depends, among other parameters, on the chosen equilibrium T_e. Notice that a second distinct equilibrium must exist provided the chosen T_e is not a double root of (5). We will return to (7) in section 5 to locate the other root and see what happens when T_e is a double root after the parameters A and B have been related to physically meaningful quantities.

The k $(2 \le k \le 8)$ equilibrium solutions of (1) may be indexed as

$$\begin{bmatrix} G_i \\ T_i \end{bmatrix} = \begin{bmatrix} 1 - \kappa T_i^4 \\ T_i \end{bmatrix} \tag{8}$$

where T_i is a solution of (7) for $i = 1, 2, ..., k$ and $T_1 = T_e$.

4 The chosen equilibrium

To study the dynamics near the equilibrium $i = 1$ in (8) we follow a standard perturbation method which can be found in Hale and Koçak (1991). We begin by translating this equilibrium to the origin. Let

$$G = y_1 + 1 - \kappa T_e^4 \tag{9}$$

$$T = y_2 + T_e. \tag{10}$$

Equations (1) with C given by (6) then become

$$\dot{\mathbf{y}} = \mathbf{A}\,\mathbf{y} + \mathbf{f}(\mathbf{y}) \tag{11}$$

where $\mathbf{y} = \begin{bmatrix} y_1 \\ y_2 \end{bmatrix}$,

$$\mathbf{A} = \begin{bmatrix} 2R\kappa T_e^4 - R - A & -B \\ 2LR\kappa T_e^4 - LR - LA - F & -LB - 4\kappa F T_e^3 \end{bmatrix} \tag{12}$$

and

$$\mathbf{f}(\mathbf{y}) = \begin{bmatrix} Ry_1^2 \\ LRy_1^2 + \kappa F y_2^4 + 4\kappa F y_2^3 T_e + 6\kappa F y_2^2 T_e^2 \end{bmatrix}. \tag{13}$$

4.1 Periodic orbits

In (11) the linearized flow ($\mathbf{f} = \mathbf{0}$) is topologically governed by the eigenvalues of the coeficient matrix $\mathbf{A}$. If the eigenvalues are of the form $\alpha \pm \imath\omega$, then for $\omega \neq 0$, all solutions will spiral toward zero for $\alpha < 0$, spiral away from zero for $\alpha > 0$, or form a periodic orbit about zero

for $\alpha = 0$ with a rotation period of $2\pi/\omega$. Clearly, however, the periodic orbits of the linear system are structurally unstable.

The nonlinear flow of (11) is much more interesting since structurally stable periodic orbits can exist for $\alpha > 0$ through Poincare-Andronov-Hopf bifurcation. While the period of these orbits is near $2\pi/\omega$, the shape and size depends upon detailed analysis of the nonlinear term $\mathbf{f}$.

The eigenvalues of $\mathbf{A}$ are $\left(tr(\mathbf{A}) \pm \sqrt{disc(\mathbf{A})}\right)/2$ where $disc(\mathbf{A}) = tr(\mathbf{A})^2 - 4det(\mathbf{A})$ is the discriminant, $tr(\mathbf{A})$ is the trace, and $det(\mathbf{A})$ is the determinant of the two dimensional matrix $\mathbf{A}$. To obtain eigenvalues of the form $\alpha \pm \imath\omega$ we write the soft parameters A and B in terms of α and ω. Specifically, if we set $tr(\mathbf{A}) = 2\alpha$ and $det(\mathbf{A}) = \alpha^2 + \omega^2$ then we have the following system

$$\begin{aligned} &2R\kappa T_e^4 - R - A - LB - 4\kappa F T_e^3 = 2\alpha \\ &4R\kappa F T_e^3 - 8R\kappa^2 T_e^7 F + 4A\kappa F T_e^3 - BF \\ &\qquad = \alpha^2 + \omega^2 \end{aligned} \tag{14}$$

which may be solved to obtain

$$\begin{aligned} B &= -\frac{16\kappa^2 F^2 T_e^6 + 8\kappa F T_e^3 \alpha + \alpha^2 + \omega^2}{F(1 + 4\kappa T_e^3 L)} \\ A &= \frac{1}{F(1 + 4\kappa T_e^3 L)} \\ &\quad \{2R\kappa T_e^4 F + 8R\kappa^2 T_e^7 FL - RF - 4RF\kappa T_e^3 L \\ &\quad -4\kappa F^2 T_e^3 - 2F\alpha + L(\alpha^2 + \omega^2)\}. \end{aligned} \tag{15}$$

It should be noted that in (15) since all parameters are real, we are choosing A and B to provide complex conjugate eigenvalues of the matrix $\mathbf{A}$. Since our goal is analyzing periodic orbits, this region in (A, B) space is advantageous.

Examining the equation for B in (15) we see for $\alpha > 0$ that $B < 0$. Since the periodic orbits require $\alpha > 0$, this provides an interpretation of the balance between enhanced melting and increased precipitation when the temperature rises, as described in Sect. 2. Thus for periodic orbits to exist, the increased precipitation must dominate the enhanced melting. The case where $B > 0$, requiring $\alpha < 0$, gives the uninteresting result of a spiral.

When (15) is put into (12) the system (11) will behave as desired. When this is done, we get

$$\begin{aligned} \mathbf{A}(\alpha, \omega) &= \frac{1}{F(1 + 4L\kappa T_e^3)} \\ &\quad \left\{ \begin{bmatrix} 4\kappa F^2 T_e^3 & 16\kappa^2 F^2 T_e^6 \\ -F^2 & -4\kappa F^2 T_e^3 \end{bmatrix} \right. \\ &\quad + \alpha \begin{bmatrix} 2F & 8\kappa F T_e^3 \\ 2LF & 8L\kappa F T_e^3 \end{bmatrix} \\ &\quad \left. + (\alpha^2 + \omega^2) \begin{bmatrix} -L & 1 \\ -L^2 & L \end{bmatrix} \right\}. \end{aligned} \tag{16}$$

Note that $\mathbf{f}(\mathbf{y})$ defined in (13) remains unchanged since A and B are coefficients of exclusively linear terms.

4.2 Stability and bifurcation

Putting (11) in a form amenable to analysis, we seek a transformation of the form

$$\mathbf{y} = \mathbf{P}\mathbf{u} \tag{17}$$

where $\mathbf{P}$ is a nonsingular matrix such that

$$\mathbf{P}^{-1}\mathbf{A}\mathbf{P} = \begin{bmatrix} \alpha & \omega \\ -\omega & \alpha \end{bmatrix}. \tag{18}$$

To calculate the transformation matrix $\mathbf{P}$ we determine the eigenvectors of the matrix $\mathbf{A}$. Recall that if a matrix has eigenvalues $\alpha \pm \imath\omega$, then the eigenvectors are of the form $\xi_\mathbf{r} \pm \imath\xi_\mathbf{i}$. Then we form the transformation matrix by setting $\mathbf{P} = [\xi_\mathbf{r} \mid \xi_\mathbf{i}]$. Having done this, we see that

$$\begin{aligned} \mathbf{P} &= \begin{bmatrix} -4\kappa F^2 T_e^3 & 0 \\ F^2 & 0 \end{bmatrix} \\ &\quad + \alpha \begin{bmatrix} 4L\kappa F T_e^3 - F & 0 \\ -2LF & 0 \end{bmatrix} \\ &\quad + \omega \begin{bmatrix} 0 & -F(1 + 4\kappa T_e^3 L) \\ 0 & 0 \end{bmatrix} \\ &\quad + (\alpha^2 + \omega^2) \begin{bmatrix} L & 0 \\ L^2 & 0 \end{bmatrix}. \end{aligned} \tag{19}$$

To study the stability of the Poincare-Andronov-Hopf bifurcation we let $\alpha = \lambda\omega$ and consider $|\lambda| \ll 1$. Transforming time to $\tau = \omega t$ the system (11) with (17) becomes

$$\mathbf{u}' = \begin{bmatrix} 0 & 1 \\ -1 & 0 \end{bmatrix} \mathbf{u} + \mathbf{g}(\mathbf{u}) \tag{20}$$

where $()' \equiv \frac{d}{d\tau}$ and

$$\mathbf{g}(\mathbf{u}) = \lambda\mathbf{u} + \frac{1}{\omega}\mathbf{P}^{-1}\mathbf{f}(\mathbf{P}\mathbf{u}). \tag{21}$$

Now we make the coordinate transformation

$$\mathbf{u} = r \begin{bmatrix} \cos\theta \\ -\sin\theta \end{bmatrix}. \tag{22}$$

From the form of $\begin{bmatrix} r' \\ \theta' \end{bmatrix}$ when (22) is used in (20), it can be shown that $\frac{d\theta}{d\tau} > 0$ in a neighborhood of $r = 0$. Consequently τ may be eliminated to obtain the one dimensional equation

$$\frac{dr}{d\theta} = \lambda r + c_2(\lambda, \theta) r^2 + c_3(\lambda, \theta) r^3 + O(r^4). \tag{23}$$

The "Big O" notation is slightly abused in that the coefficients of the higher order terms are 2π periodic dependent on θ.

The coordinate transformation to eliminate the θ dependence in the first few terms of (23) is of the form

$$r = \rho + b_2(\lambda, \theta)\rho^2 + b_3(\lambda, \theta)\rho^3 \tag{24}$$

where $b_2(\lambda,\theta)$ and $b_3(\lambda,\theta)$ are chosen to be 2π periodic in θ. When this transformation is put in (23) the resulting differential equation for ρ is

$$\begin{aligned}\frac{d\rho}{d\theta} &= \lambda\rho + \left(c_2 - \frac{db_2}{d\theta} - \lambda b_2\right)\rho^2 \\ &+ \left(c_3 + 2b_2\frac{db_2}{d\theta} - \frac{db_3}{d\theta} - 2\lambda(b_3 + {b_2}^2)\right)\rho^3 \\ &+ O(\rho^4). \end{aligned} \tag{25}$$

By requiring

$$\begin{aligned}\frac{db_2}{d\theta}(\lambda,\theta) &= c_2(\lambda,\theta) - \bar{c}_2(\lambda) \\ \frac{db_3}{d\theta}(\lambda,\theta) &= c_3(\lambda,\theta) + 2\,b_2(\lambda,\theta)\frac{db_2(\lambda,\theta)}{d\theta} - \bar{c}_3(\lambda)\end{aligned} \tag{26}$$

where the constants $\bar{c}_2(\lambda)$ and $\bar{c}_3(\lambda)$ represent the "average" of the coefficients $c_2(\lambda,\theta)$ and $c_3(\lambda,\theta)$ by

$$\begin{aligned}\bar{c}_2(\lambda) &= \frac{1}{2\pi}\int_0^{2\pi} c_2(\lambda,s)\,ds \\ \bar{c}_3(\lambda) &= \\ &\frac{1}{2\pi}\int_0^{2\pi}\left(c_3(\lambda,s) + 2\,b_2(\lambda,\theta)\frac{db_2(\lambda,\theta)}{d\theta}\right)ds \\ &= \frac{1}{2\pi}\int_0^{2\pi} c_3(\lambda,s)\,ds\end{aligned} \tag{27}$$

we obtain the desired transformation.

From the symmetry in forming (23) from a two dimensional equation, $\bar{c}_2 = 0$. With the transformation (24) and the defintion (26) we obtain

$$\frac{d\rho}{d\theta} = \lambda\rho + (\bar{c}_3 + O(\lambda))\,\rho^3 + O(\rho^4). \tag{28}$$

We analytically determine $\bar{c}_3$ to be

$$\begin{aligned}\bar{c}_3 &= \left(\frac{\kappa T_e}{1+4\,L\kappa T_e^3}\right)\left(\frac{L^2\omega^2+F^2}{2\,\omega^3}\right) \\ &\{\ 3\,L^2\left(10L\kappa FT_e^3 + T_eR + F\right)\omega^4 \\ &+ \left(48\,L^2F^2\kappa^2T_e^7R - 72\,L^2F^3\kappa^2T_e^6\right. \\ &\quad +8\,LF\kappa T_e^5R^2 - 12\,LF^2\kappa T_e^4R \\ &\quad \left.+30\,LF^3\kappa T_e^3 + 2\,FT_e^2R^2 + 3\,F^3\right)\omega^2 \\ &+ 8\,\kappa^2T_e^6F^3\left(2\,T_eR - 3\,F\right)\left(8\,LR\kappa T_e^4\right. \\ &\quad \left.+2\,T_eR + 3\,F\right)\ \} + O(\lambda).\end{aligned} \tag{29}$$

The stability of (28) is determined by the sign of $\bar{c}_3$. Parameter ranges such that $\bar{c}_3 < 0$ will give rise to a stable nontrivial periodic orbit about the origin. Letting a represent the radius of the periodic orbit in $\mathbf{u}$ coordinates, we have the approximate bifurcation curve

$$\lambda(a) = -\bar{c}_3\,a^2 + O(a^3)\ ,\ a \to 0. \tag{30}$$

5 The second equilibrium

Since the polynomial (5) is of even order and we chose one real root using (6), there must exist a second real root. In this section, we find an asymptotic approximation for this second equilibrium. With an analytic approximation for the second equilibrium we may analyze the topological character of the dynamics near this equilibrium. Also, the proximity of this equilibrium with respect to the chosen equilibrium is of interest.

5.1 Approximation

In choosing an expansion parameter, we notice that setting $\alpha = \omega = 0$ in (15) and putting this in (7) causes T_e to be a double root. This can be seen by factoring the resulting polynomial to obtain

$$\begin{aligned}(T-T_e)^2\{ &- R\kappa^2T^6 - 2\,R\kappa^2T_eT^5 - 3\,R\kappa^2T_e^2T^4 \\ &-4\,R\kappa^2T_e^3T^3 - \frac{T_e^3\left(12\,LR\kappa T_e^4+3\,RT_e+4\,F\right)\kappa^2}{1+4\,\kappa T_e^3L}T^2 \\ &-\frac{2\,T_e^4\left(4\,LR\kappa T_e^4+RT_e+4\,F\right)\kappa^2}{1+4\,\kappa T_e^3L}T \\ &-\frac{T_e^5\left(12\,F+RT_e+4\,LR\kappa T_e^4\right)\kappa^2}{1+4\,\kappa T_e^3L}\ \} = 0.\end{aligned} \tag{31}$$

Clearly with the choice of $\alpha = \omega = 0$ the Jacobi matrix evaluated at the first equilibrium is singular. However, this does provide us with convienent expansion parameters. We will use the approximate radius of the orbit about the first equilibrium, a, as an expansion parameter instead of α so we can relate the expansions to the phase dynamics. The coefficients of a in the expansion are then approximated for small ω.

To obtain an expansion in a for T_2 in (8), we substitute (15) in (7) using (30). Recalling that $\alpha = \lambda\omega$ and $\bar{c}_3$ is given from (29), we let

$$T_2 = \Gamma_0 + \Gamma_1\,a + \Gamma_2\,a^2 + O(a^3) \tag{32}$$

and see that Γ_0 is the root of the seventh order polynomial

$$\begin{aligned}&-R\kappa^2T^7 - R\kappa^2T_eT^6 - R\kappa^2T_e^2T^5 - R\kappa^2T_e^3T^4 \\ &+\frac{\kappa\left(R\kappa T_e^4F+4\,R\kappa^2T_e^7FL+L\omega^2-4\,\kappa F^2T_e^3\right)}{F(1+4\,\kappa T_e^3L)}T^3 \\ &+\frac{\kappa T_e\left(R\kappa T_e^4F+4\,R\kappa^2T_e^7FL+L\omega^2-4\,\kappa F^2T_e^3\right)}{F(1+4\,\kappa T_e^3L)}T^2 \\ &+\frac{\kappa T_e^2\left(R\kappa T_e^4F+4\,R\kappa^2T_e^7FL+L\omega^2-4\,\kappa F^2T_e^3\right)}{F(1+4\,\kappa T_e^3L)}T \\ &+\frac{12\,\kappa^2F^2T_e^6+\omega^2+\kappa^2FT_e^7R+4\,\kappa^3FT_e^{10}LR+\omega^2\kappa T_e^3L}{F(1+4\,\kappa T_e^3L)} = 0.\end{aligned} \tag{33}$$

Assumming now that

$$\Gamma_0 = \gamma_0 + \gamma_1\,\omega + \gamma_2\,\omega^2 + O(\omega^3) \tag{34}$$

we obtain

$$\begin{aligned}\Gamma_0 &= T_e + \frac{\left(1+4\,\kappa T_e^3L\right)}{8\,FT_e^5\kappa^2\left(2\,RT_e + 8\,LR\kappa T_e^4 + 3\,F\right)}\omega^2 \\ &+ O(\omega^4).\end{aligned} \tag{35}$$

Now using (35) in (32) the terms Γ_1 and Γ_2 can be found from (7) with (15), (30), and (29). With the resultant approximation of T_2, G_2 is found using (8), and we obtain the approximation for the second equilibrium as

$$\begin{aligned}\mathbf{y}_{eq2} &\equiv \begin{bmatrix} G_2 \\ T_2 \end{bmatrix} - \begin{bmatrix} 1-\kappa T_e^4 \\ T_e \end{bmatrix} \\ &= \frac{(1+4\kappa T_e^3 L)}{(2RT_e+8LR\kappa T_e^4+3F)} \begin{bmatrix} \frac{-1}{2\kappa T_e^2 F} \\ \frac{1}{8FT_e^5\kappa^2} \end{bmatrix} \omega^2 \\ &+ \frac{3F^4(2RT_e-3F)}{2RT_e+8LR\kappa T_e^4+3F} \begin{bmatrix} -\kappa T_e^2 \\ \frac{1}{4T_e} \end{bmatrix} a^2 \\ &+ \begin{bmatrix} O(\omega^4)+O(\omega^2a^2) \\ O(\omega^4)+O(\omega^2a^2) \end{bmatrix}. \end{aligned} \tag{36}$$

5.2 Saddle character

We may now use the approximation (36) to evaluate properties of the linearization of (1) about the second equilibrium. Instead of re-translating to the origin as in (9), we take advantage of the form of (36) and use the coordinates $\mathbf{y}$ already in use. This should avoid confusion about which origin is being discussed, as $\mathbf{y} = \mathbf{0}$ will still be the chosen equilibrium.

The Jacobi matrix of (11) is

$$\begin{aligned}&\mathbf{J}(\mathbf{y}) = \mathbf{A} \\ &+ \begin{bmatrix} -2Ry_1 & 0 \\ -2LRy_1 & -4\kappa F y_2^3 - 12\kappa F y_2^2 T_e - 12\kappa F y_2 T_e^2 \end{bmatrix}\end{aligned} \tag{37}$$

where the matrix $\mathbf{A}$ is defined in (16).

Using (36), we approximate the discriminant of $\mathbf{J}$ to determine the nature of the eigenvalues using the lowest order terms in a and ω. Specifically, we see that

$$\begin{aligned}&disc\left(\mathbf{J}\left(\mathbf{y}_{eq2}\right)\right) = 4\omega^2 \\ &- \left(8\left(2RT_e - 3F\right)^2 F^4\kappa^2 T_e^4\right) a^2 \\ &+ O(\omega^4) + O(\omega^2 a^2).\end{aligned} \tag{38}$$

So we will expect two real eigenvalues for fixed ω as $a \to 0$. Forming the rest of the eigenvalues, we have

$$\begin{aligned}\mu_\pm &= \pm\omega + \frac{(1+4\kappa T_e^3 L)(2RT_e-3F)}{4\kappa T_e^3(2RT_e+8LR\kappa T_e^4+3F)F}\omega^2 \\ &+ O(\omega^4) + O(\tfrac{a^2}{\omega^2}).\end{aligned} \tag{39}$$

Clearly this equilibrium has a saddle character as one eigenvalue is positive and one is negative. With an equilibrium of this type, the natural structure of the one dimensional invariant manifold provides borders for the phase flow. These inflowing and outflowing (stable and unstable) manifolds may intersect to form a homoclinic orbit.

5.3 Stability

Homoclinic orbits for conservative or Hamiltonian systems may be written down exactly when they exist. However this luxury is not available for general systems and numerical integration becomes the basis for determining the existence of such an orbit. In seeking such an orbit, it is helpful to know the stability properties. From Chow and Hale (1982) it is shown that if the trace of the matrix $\mathbf{J}$ in (37) is negative, then the homoclinic orbit, if it exists, is asymptotically stable. Analyzing the trace of (37) evaluated at (36) we see that

$$\begin{aligned}&tr\left(\mathbf{J}\left(\mathbf{y}_{eq2}\right)\right) = \frac{(1+4\kappa T_e^3 L)(2RT_e-3F)}{2\kappa T_e^3(2RT_e+8LR\kappa T_e^4+3F)F}\omega^2 \\ &- \frac{8T_e^7\kappa^3F^5(2RT_e-3F)\left(2RT_e+8LR\kappa T_e^4+3F\right)}{1+4\kappa T_e^3 L}\frac{a^2}{\omega^2} \\ &+ O(\omega^4) + O(a^2).\end{aligned} \tag{40}$$

Noting that all parameters are positive, it follows that the trace is negative for small ω as $a \to 0$ if $T_e < \frac{3F}{2R}$.

6 Parameter analysis

Qualitative model behavior may be obtained by analyzing the results of the previous sections in terms of the soft parameters. It is stressed, however, that this qualitative behavior may easily be related to any of the other parameters. This is a benefit of analytic approximation.

The three soft parameters governing physical quantities are ω for the period, T_e for the equilibrium temperature, and a for the deviation from equilibrium. The original formulation provides an interpretation of ω and T_e. Since a is radius of the orbit in $\mathbf{u}$ coordinates, the deviations of T and G from their equilibrium values on the periodic orbit requires a transformation to $\mathbf{y}$ coordinates.

The results of this section are only approximate and should be used in conjunction with a physical interpretation of parameters. Although the assumption that $a \to 0$ in the derivations places an inherent restriction on the radius of the periodic orbit, this "near equilibrium" analysis is useful in determining parameter interplay.

For the remaining parameters, we will use the values given by Posmentier (1990)

$$\begin{aligned}L &= 20\ ^\circ\mathbf{K} \\ K &= 1.07 * 10^{-10}\ \frac{1}{^\circ\mathbf{K}\,\mathbf{yr}} \\ F &= .43395\ \frac{^\circ\mathbf{K}}{\mathbf{yr}} \\ R &= 8 * 10^{-5}\ \frac{1}{\mathbf{yr}}.\end{aligned} \tag{41}$$

Since the units of A and C are $1/\mathbf{yr}$ and the units of B are $1/(^\circ\mathbf{K}\,\mathbf{yr})$, we see that α and ω are in $1/\mathbf{yr}$. Both components of the vector $\mathbf{u}$ and the radius a are in units of $\mathbf{yr}^2/^\circ\mathbf{K}$.

6.1 Minimum period

Treating $\bar{c}_3$ in (29) as a function of ω we may determine an approximate maximum ω value for stability. From

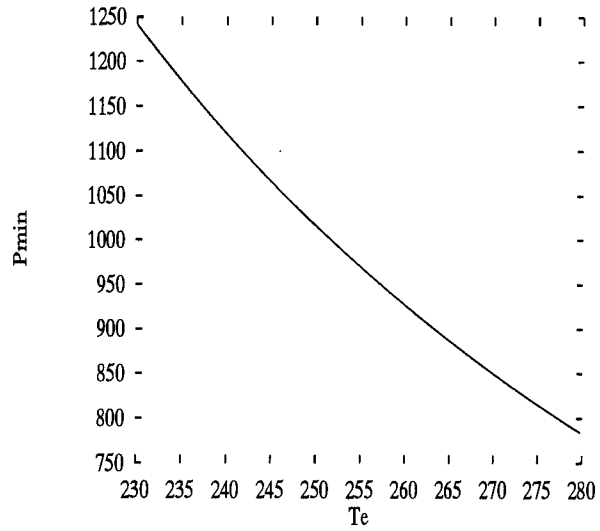

Fig. 1. Minimum stable period P_{min} (**yr**) plotted verses equilibrium temperature T_e (°**K**).

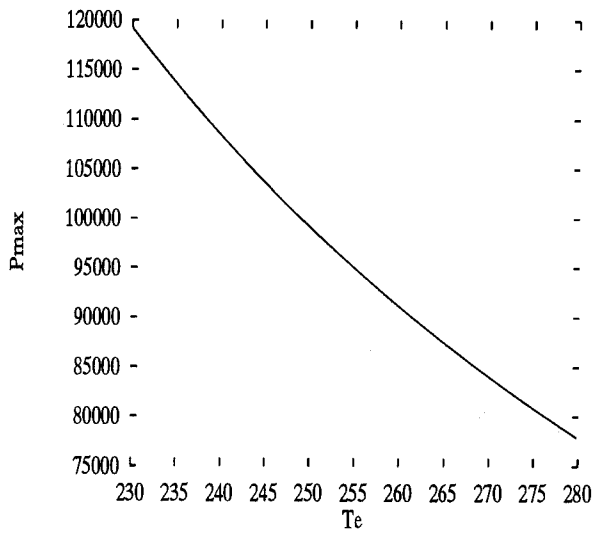

Fig. 2. Maximum period P_{max} (**yr**) plotted verses equilibrium temperature T_e (°**K**) with $a = 0.1\,\mathbf{yr}^2/°\mathbf{K}$.

(29), we see that $\bar{c}_3 = 0$ only at the roots of the quadratic in ω^2

$$\begin{aligned} &3L^2\left(10L\kappa FT_e^3 + T_eR + F\right)\omega^4 + \\ &\left(48\,L^2F^2\kappa^2T_e^7R - 72\,L^2F^3\kappa^2T_e^6 + 8\,LF\kappa T_e^5R^2 - \right. \\ &\left. 12\,LF^2\kappa T_e^4R + 30\,LF^3\kappa T_e^3 + 2\,FT_e^2R^2 + 3\,F^3\right)\omega^2 \\ &+8\,\kappa^2T_e^6F^3\left(2\,T_eR - 3\,F\right)\left(8\,LR\kappa T_e^4 + 2\,T_eR + 3\,F\right) \\ &= 0. \end{aligned} \tag{42}$$

The maximum value of ω that produces a stable periodic orbit is then

$$\begin{aligned} \omega_{max}^2 = &\tfrac{1}{60\,\kappa FT_e^3L^3 + 6\,L^2RT_e + 6\,L^2F}\left\{-3\,F^3\right. \\ &-48\,L^2\kappa^2T_e^7RF^2 + 72\,L^2\kappa^2F^3T_e^6 - 8\,LR^2\kappa T_e^5F \\ &+12\,LR\kappa T_e^4F^2 - 30\,L\kappa F^3T_e^3 - 2\,R^2FT_e^2 \\ &+F\left(1 + 4\,\kappa T_e^3L\right)\left(\right. 816\,L^2\kappa^2F^2R^2T_e^8 \\ &-1008\,L^2\kappa^2RF^3T_e^7 - 324\,L^2\kappa^2F^4T_e^6 \\ &+48\,LR^3\kappa FT_e^6 - 72\,L\kappa F^2R^2T_e^5 \\ &+72\,LR\kappa F^3T_e^4 - 4\,R^4T_e^4 - 108\,L\kappa F^4T_e^3 \\ &\left.\left. -12\,R^2F^2T_e^2 - 9\,F^4\right)^{1/2}\right\}. \end{aligned} \tag{43}$$

Plotting $P_{min} = 2\pi/\omega_{max}$ verses T_e in Fig. 1 we obtain minimum stable periods as a function of the chosen equilibrium temperature. Notice that this minimum period is independent of the radius a.

6.2 Maximum period

If the periodic orbit intersects the second equilibrium we expect a bifurcation to occur. So we may obtain a minimum frequency ω_{min} of the periodic orbit in terms of a by using **u** coordinates, since the orbit in this coordinate system is a circle. This intersection is determined by solving the equation

$$a = \left\|\mathbf{P}^{-1}\left(\mathbf{y}_{eq2}\right)\right\|_{\mathbf{u}} \tag{44}$$

where $\|\mathbf{u}\|_{\mathbf{u}} = \sqrt{u_1^2 + u_2^2}$ is the Euclidean norm in **u** coordinates. When this is done, we get the approximation

$$\begin{aligned} \omega_{min}^2 = &\tfrac{8\,F^3T_e^5\kappa^2\left(2\,RT_e + 8\,LR\kappa T_e^4 + 3\,F\right)}{1 + 4\,\kappa T_e^3L}a \\ &+O(a^2) + O(\omega^4). \end{aligned} \tag{45}$$

In Fig. 2 we set $a = 0.1\,\mathbf{yr}^2/°\mathbf{K}$ and plot $P_{max} = 2\pi/\omega_{min}$ as a function of equilibrium temperature T_e. Notice that this period is governed in magnitude by a factor of $1/\sqrt{a}$.

6.3 Deviation from equilibrium

We have determined the approximate $\lambda(a)$ giving a periodic orbit of radius a in **u** coordinates by (30). However, to relate this to physically meaningful coordinates, we need to determine how this orbit maps to **y** coordinates. Using $\mathbf{y} = \mathbf{Pu}$ and $r = a$ in (22) we see that

$$\begin{aligned} \mathbf{y}_{periodic} = &\begin{bmatrix} -4\,\kappa F^2T_e^3 + L\omega^2 \\ L^2\omega^2 + F^2 \end{bmatrix} a\cos(\theta) \\ &+\begin{bmatrix} F\omega + 4\,F\omega\,\kappa T_e^3L \\ 0 \end{bmatrix} a\sin(\theta) + \begin{bmatrix} O(a^3) \\ O(a^3) \end{bmatrix} \end{aligned} \tag{46}$$

where $\theta = \theta(t)$. The approximate maximum deviation from equilibrium temperature is then

$$T_{max} = \left(L^2\omega^2 + F^2\right)a \tag{47}$$

and the approximate maximum deviation from glaciation equilibrium is

$$G_{max} = T_{max}\sqrt{\frac{16\,\kappa^2F^2T_e^6 + \omega^2}{L^2\omega^2 + F^2}}. \tag{48}$$

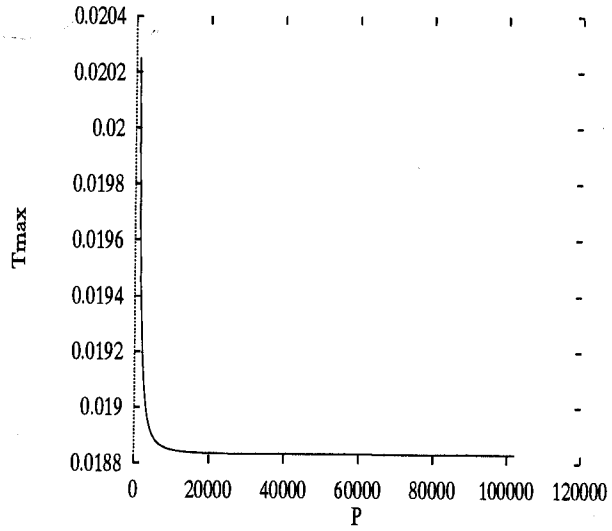

Fig. 3. Maximum temperature deviation from equilibrium T_{max} (°K) plotted from P_{min} (yr) to P_{max} (yr) with T_e = 246 °K and $a = 0.1\,\mathbf{yr}^2/°\mathbf{K}$.

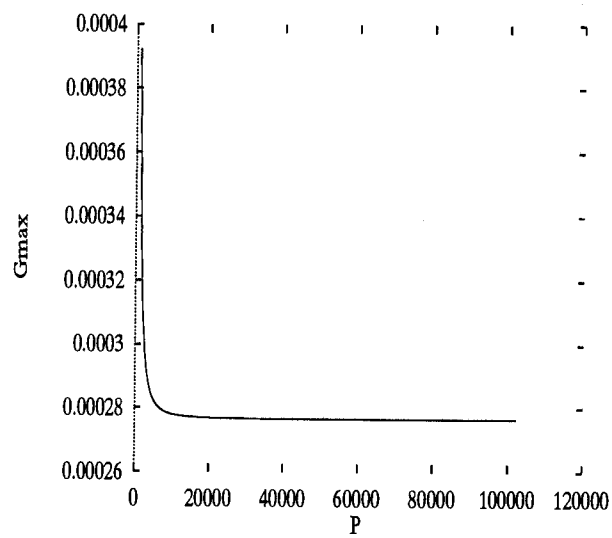

Fig. 4. Maximum glaciation deviation from equilibrium G_{max} plotted from P_{min} (yr) to P_{max} (yr) with T_e = 246 °K and $a = 0.1\,\mathbf{yr}^2/°\mathbf{K}$.

In Fig. 3 and Fig. 4 we set $a = 0.1\,\mathbf{yr}^2/°\mathbf{K}$ and T_e = 246 °K (equilibrium glaciation $G_1 = 1 - \kappa T_e^4 = 0.0970$) to plot these deviations from P_{min} to P_{max}.

7 Numerical solutions

We now demonstrate the bifurcation of the periodic orbit to a homoclinic orbit by examining the behavior of the invariant sets of the system, namely the periodic orbit about the chosen equilibrium and the saddle manifolds of the second equilibrium. These solutions govern the topology of the phase space. A mean radiation equilibrium temperature of T_e = 246 °K is used as in Posmentier (1990).

The radius of the periodic orbit in **u** coordinates is set to $a = 0.1\,\mathbf{yr}^2/°\mathbf{K}$ and we integrate the inflowing and outflowing manifolds of the second equilibrium for various ω values. As ω approaches ω_{min}, the radius of the periodic orbit approaches the second equilibrium with saddle character and we expect a bifurcation. For the parameters chosen, we have $\omega_{min} = 2\,\pi/102,681\mathbf{yr}$.

Integrations were done (in **y** coordinates) with the LSODA routine of the public domain software ODEPACK using initial conditions from Maple. Initial conditions for the periodic orbits were obtained by (46). The saddle manifolds of the second equilibrium were determined by first locating the equilibrium numerically and then calculating the eigenvalues and eigenvectors of the matrix (37) at the determined equilibrium. Then the outflowing manifolds were integrated in positive time using small (10^{-5} to 10^{-9}) displacements from the second equilibrium in the direction of the eigenvectors corresponding to the positive eigenvalue. The inflowing manifolds were integrated in negative time along the eigenvectors corresponding to the negative eigenvalue. Trajectories integrated in positive time are solid lines, while dashed lines correspond to trajectories integrated in negative time. Arrows indicate the direction of the flow for positive time.

In Fig. 5 the periodic orbit is shown in **y** coordinates for $\omega = 2\,\pi/20,000\mathbf{yr}$. The same orbit in **u** coordinates in shown in Fig. 6. The stable and unstable manifolds of the second equilibrium with this choice of ω is then shown in Fig. 7.

In Fig. 8 we decrease ω to $2\,\pi/50,000\mathbf{yr}$ and see the periodic orbit approach the saddle manifolds. When $\omega = 2\,\pi/120,000\mathbf{yr}$ the inflowing and outflowing manifolds cross each other, as seen in Fig. 9. Since the manifolds depend continuously upon ω, we conclude they must intersect for some value between $2\,\pi/50,000\mathbf{yr}$ and $2\,\pi/120,000\mathbf{yr}$ to form a homoclinic orbit.

Finding the exact value of ω via computer experiments is not, in general, possible. We may get very close by observing the crossing of the inflowing and outflowing manifolds and adjusting ω appropriately, a bisection technique of sorts. It should be clear that even if such a value of ω were determined to arbitrary precision, computer roundoff will not allow a simulation of a true homoclinic orbit. For the parameters selected, the inflowing and outflowing manifolds intersect between $\omega = 2\,\pi/89,276\mathbf{yr}$ and $\omega = 2\,\pi/89,277\mathbf{yr}$. Fig. 10 shows the approximate homoclinic orbit.

When $\omega = 2\,\pi/89,276\mathbf{yr}$, the local phase space topology is that of Fig. 7 and Fig. 8 where the periodic orbit attracts in positive time and the attracting region for

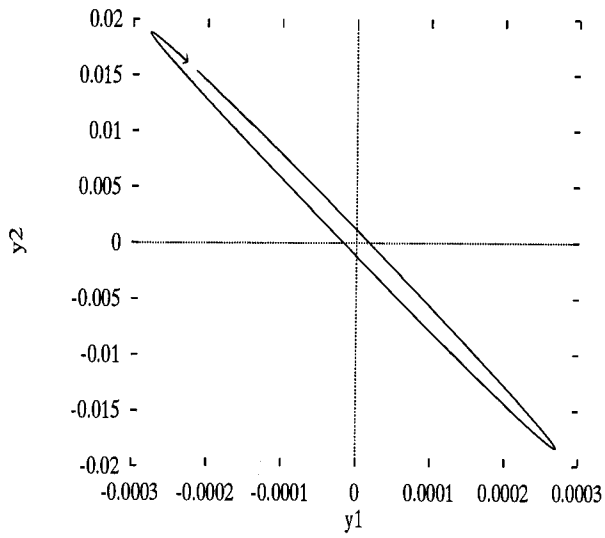

Fig. 5. Periodic orbit in **y** coordinates y_2 (°**K**) vs y_1 (*unitless*) for $\omega = 2\pi/20{,}000$**yr**.

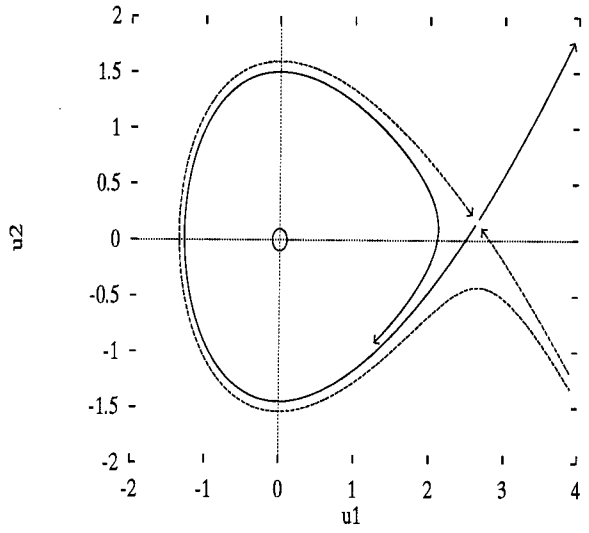

Fig. 7. Inflowing and outflowing manifolds of the second equilibrium in **u** (**yr**^{2}/°**K**) coordinates for $\omega = 2\pi/20{,}000$**yr**. The attracting region for the periodic orbit is bounded by the two inflowing manifolds.

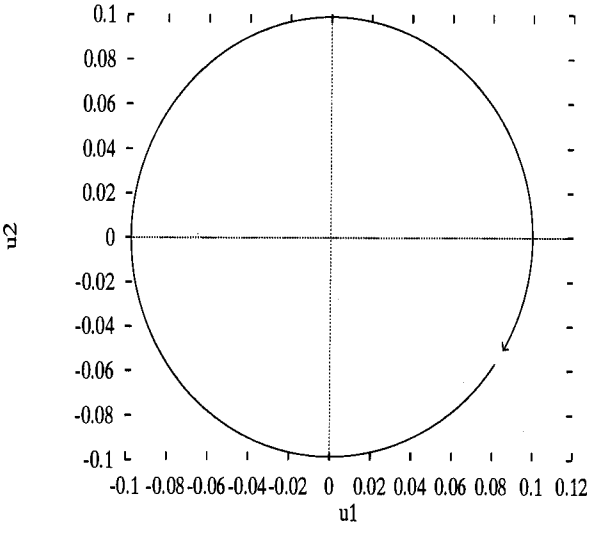

Fig. 6. Periodic orbit in **u** (**yr**^{2}/°**K**) coordinates for $\omega = 2\pi/20{,}000$**yr**.

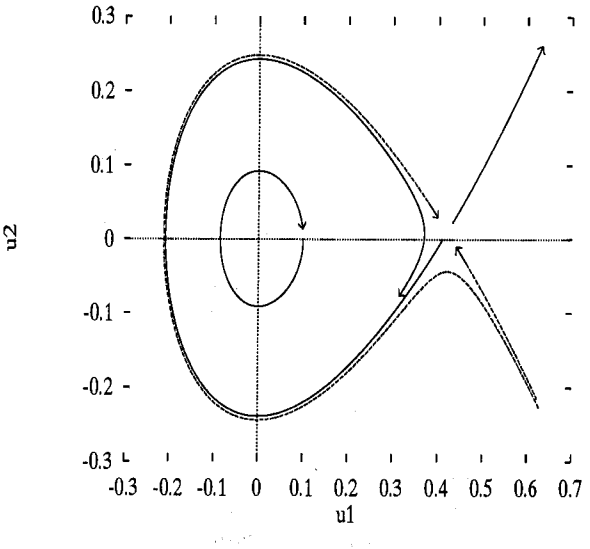

Fig. 8. Inflowing and outflowing manifolds of the second equilibrium and the periodic orbit about the first equilibrium in **u** (**yr**^{2}/°**K**) coordinates for $\omega = 2\pi/50{,}000$**yr**.

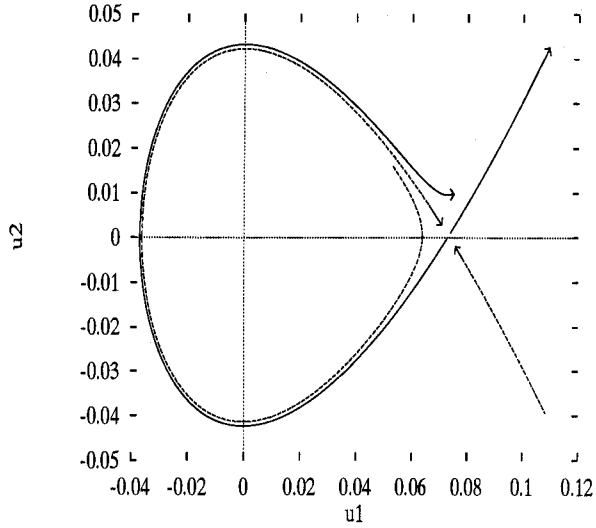

Fig. 9. Crossing of the inflowing and outflowing manifolds of the second equilibrium in $\mathbf{u\,(yr^2/°K)}$ coordinates for $\omega = 2\pi/120{,}000\mathbf{yr}$.

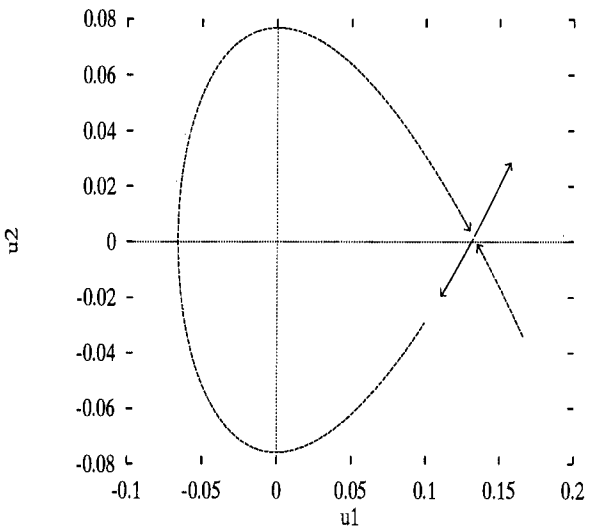

Fig. 10. Inflowing and outflowing manifolds in $\mathbf{u\,(yr^2/°K)}$ coordinates at the approximate intersection value of $\omega = 2\pi/89277\mathbf{yr}$.

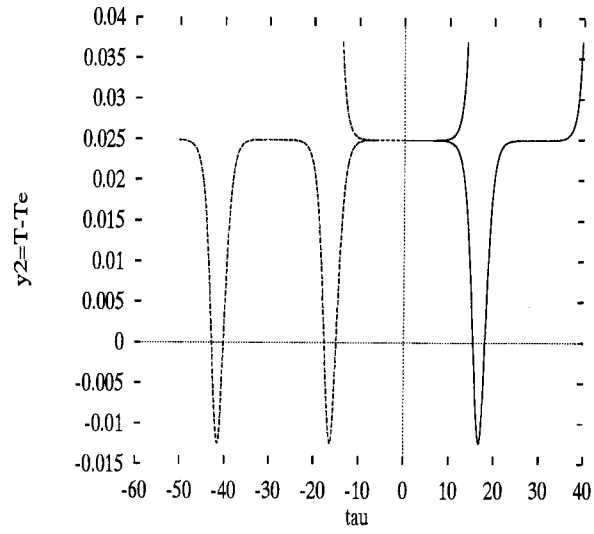

Fig. 11. The time series y_2 (°K) vs τ (*unitless*) of the saddle manifolds for $\omega = 2\pi/89277\mathbf{yr}$. The periodic orbit bifurcating from the homoclinic orbit attracts in negative time.

this periodic orbit is bounded between the two inflowing manifolds. The time series for all four of the saddle manifolds with this ω value are shown in Fig. 12.

When $\omega = 2\pi/89,277\mathbf{yr}$, the local phase space topology is that of Fig. 9 where the periodic orbit attracts in negative time and solutions leave this orbit in positive time through the region bounded by the two outflowing manifolds. The time series for all four of the saddle manifolds with this ω value are shown in Fig. 11.

Details of the types of structures that bifurcate from the intersection of inflowing and outflowing manifolds can be found in Chow and Hale (1982).

8 Conclusions

Inroducing periodic orbits about a constant equilibrium as in Sect. 4 is an established procedure. The resulting local phase topology, however, gives a more complete picture of the dynamics. The existance and proximity of the adjacent equilibrium with saddle character in Sect. 5 is interesting.

The location of this second equilibrium provides a bound on the radius of the periodic orbit. The behavior of the saddle manifolds of this second equilibrium gives a region of attraction to the periodic orbit. Notice how the size of the region of attraction shrinks as the period becomes large.

The homoclinic orbit, as seen when the saddle manifolds intersect, could be the cause of the chaotic dynamics seen by Posmentier (1990). It is known that two dimensional homoclinic orbits under time dependent perturbations can produce chaotic dynamics, as in

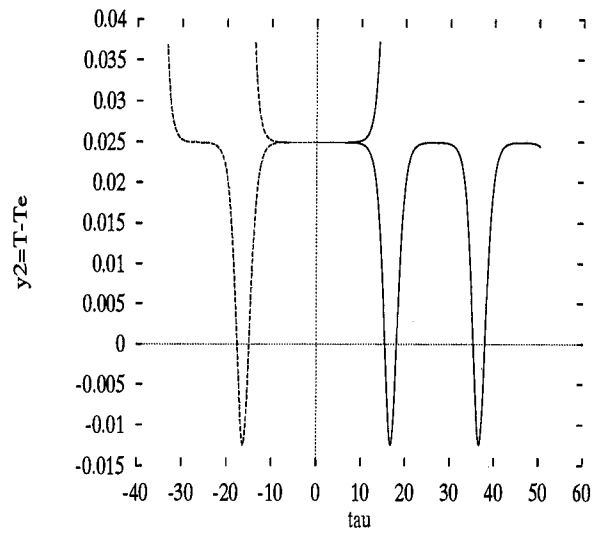

Fig. 12. The time series y_2 (°K) vs τ (*unitless*) of the saddle manifolds for $\omega = 2\pi/89276$yr. The periodic orbit bifurcating from the homoclinic orbit attracts in positive time.

the forced Duffing equation.

Although the physics described here is extremely simple we are able to determine parameter ranges that produce very different model behavior. The analytic results of Sect. 6 provide for general trends of the model and are used to gain insight into parameter relationships. Future work could consist of determining ranges of the other parameters via higher dimensional bifurcation manifolds.

A more realistic model could incorporate the parameters as variables and build upon this simple model. Issues such as the onset of chaos, the predictability of transients, and the climate response to perodic and stochastic forcing could be addressed in this formulation.

Acknowledgements. The Office of Navel Research provided support for this research through contract N00014-91-1560 to Old Dominion University. A.D. Kirwan also acknowledges the support of the Samuel L. and Fay M. Slover endowment. Thanks are extended to Wayne K. Schroll for providing the ODEPACK library in a usable form.

References

Chow, S.-N. and Hale, J. K., *Methods of Bifurcation Theory.* Springer-Verlag, New York, 1982.

Hale, J. K. and Koçak, H., *Dynamics and Bifurcations.* Springer-Verlag, New York, 1991.

Posmentier, E. S., Periodic, quasiperiodic, and chaotic behavior in a toy climate model, *Annales Goephysicae*, *8*(11), 781–790, 1990.